Sensorless Synchronous Reluctance Motor Drives: A Sensitivity Analysis Framework and Design to Achieve Stator Resistance Immunity

Sensorless Synchronous Reluctance Motor Drives: A Sensitivity Analysis Framework and Design to Achieve Stator Resistance Immunity

Anantaram Varatharajan
Department of Energy
Politecnico di Torino
Torino, Italy
anantaram.varatharajan@polito.it

Gianmario Pellegrino
Department of Energy
Politecnico di Torino
Torino, Italy
gianmario.pellegrino@polito.it

***Abstract*—The paper presents a generic framework for analysis of stator resistance variation in the stability of position observers. The adverse impact of the resistance error on the active flux based sensorless control is studied. A new technique, Adaptive Projection vector for Position error estimation (APP), is proposed to have inherent immunity to resistance errors; in addition, a resistance adaption is devised for accurate estimation of stator flux and torque. The observers are subjected to stability analysis. The instability of active flux control and the merits of the proposed technique are experimentally demonstrated on a 1 kW synchronous reluctance machine test bench.**

***Index Terms*—Sensorless control, stator resistance adaption, active flux, synchronous reluctance machine, hybrid flux observer.**

I. Introduction

Owing to the saliency of synchronous reluctance (SyR) machine, the position and speed estimation without an encoder or resolver becomes realizable. The literature contains numerous works on high frequency signal injection methods in different reference frames for operation at low and zero speeds region; [1] presents a comprehensive review of high frequency injection techniques. Fundamental wave excitation based approach is preferred at medium and high speeds; fusion methods are available for smooth transition between the two methods [2]. The proposed technique falls in the second category and can easily be augmented with high frequency injection schemes.

The flux and position observers are highly susceptible to resistance variation at low speeds, leading to large steady-state errors and even instability. To circumvent this, several methods have been explored: stator resistance observer for salient synchronous machines is proposed in [3]; sliding mode observer is developed in [4]; a recursive least square approach is resorted to identify resistance online in [5].

The section II and III introduces notations and establishes the generic framework for analysis of sensorless control system. The section IV and V presents the main contributions of the paper, they are as follows:

- The instability of active flux based sensorless control owing to resistance errors is expounded.
- A position observer based on Adaptive Projection vector for Position error estimation (APP) is developed that is immune to resistance error for operating points respecting Maximum Torque Per Amps (MTPA) law.
- The immunity also extends to the voltage error due to non-ideal compensation of inverters as the fundamental component of voltage error is in phase with the stator current [6].
- A stator resistance adaption is developed to alleviate the steady-state position error at non-MTPA operating points; furthermore, it aids in accurate estimation of stator flux and torque.
- The observers are subjected to stability analysis.

The section VI evaluates the performance of proposed method with a 1.1 kW SyR motor drive.

II. Motor Model

The electrical rotor position is θ and the electrical angular speed is $\omega = s\,\theta$. Estimated vectors are represented by the superscript $\hat{}$. The orthogonal rotational matrix is $\mathbf{J} = \left[\begin{smallmatrix} 0 & -1 \\ 1 & 0 \end{smallmatrix}\right]$ and $\mathbf{I}$ is the identity matrix.

The machine model is expressed in coordinates of estimated rotor reference frame, denoted by subscript $\hat{dq}$, whose d-axis is at $\hat{\theta} = \theta - \tilde{\theta}$, where $\tilde{\theta}$ is the position error. The speed error is symbolized by $\tilde{\omega} = \omega - \hat{\omega}$. Real space vectors will be used; for

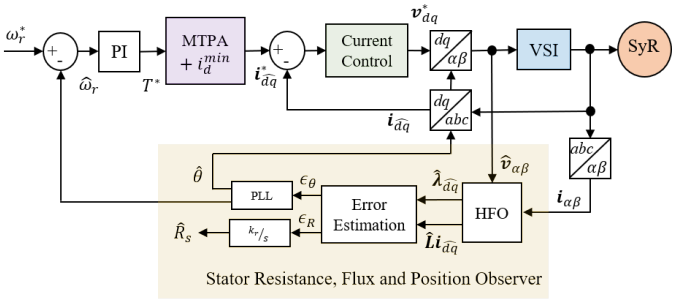

Fig. 1. Control system overview revealing the hybrid flux observer (HFO) augmented with stator resistance, position and speed adaption

example, the stator current is $\boldsymbol{i}_{\hat{d}\hat{q}} = [i_{\hat{d}}, i_{\hat{q}}]^{\mathrm{T}}$ where $i_{\hat{d}}$ and $i_{\hat{q}}$ are the vector components in estimated rotor reference frame. Space vectors in stationary reference frame are denoted by subscript $\alpha\beta$.

A. Mathematical Model of the SyR Machine

The voltage equation of a SyR machine is expressed in (1) where R_s is the stator resistance and $\boldsymbol{\lambda}_{\hat{d}\hat{q}}$ is the stator flux linkage.

$$s\,\boldsymbol{\lambda}_{\hat{d}\hat{q}} = \boldsymbol{v}_{\hat{d}\hat{q}} - R_s \boldsymbol{i}_{\hat{d}\hat{q}} - \hat{\omega}\,\mathbf{J}\,\boldsymbol{\lambda}_{\hat{d}\hat{q}} \tag{1}$$

The stator flux linkage and its time-derivative in terms of the incremental inductance $\boldsymbol{l}$ and apparent inductance $\boldsymbol{L}$ matrices are expressed in (2).

$$\boldsymbol{\lambda}_{\hat{d}\hat{q}} = \mathrm{e}^{\mathbf{J}\tilde{\theta}}\,\boldsymbol{L}\,\mathrm{e}^{-\mathbf{J}\tilde{\theta}}\,\boldsymbol{i}_{\hat{d}\hat{q}} \tag{2a}$$

$$s\,\boldsymbol{\lambda}_{\hat{d}\hat{q}} = (s\,\tilde{\theta})\,\mathbf{J}\,\boldsymbol{\lambda}_{\hat{d}\hat{q}} + \mathrm{e}^{\mathbf{J}\tilde{\theta}}\,\boldsymbol{l}\,s\left(\mathrm{e}^{-\mathbf{J}\tilde{\theta}}\,\boldsymbol{i}_{\hat{d}\hat{q}}\right) \tag{2b}$$

The components of the inductance matrices are shown in (3) where where l_d, l_q represents the incremental inductance along direct d and quadrature q axis respectively while l_{dq} is the cross-saturation term. Apparent inductance are defined likewise. All quantities are a function of $\boldsymbol{i}_{dq}$

$$\boldsymbol{l}(\boldsymbol{i}_{dq}) = \begin{bmatrix} l_d & l_{dq} \\ l_{dq} & l_q \end{bmatrix} \qquad \boldsymbol{L}(\boldsymbol{i}_{dq}) = \begin{bmatrix} L_d & 0 \\ 0 & L_q \end{bmatrix} \tag{3}$$

The estimated electromagnetic torque is given by (4) where p is the number of pole pairs.

$$\hat{T} = \frac{3p}{2}(\boldsymbol{\lambda}_{\hat{d}\hat{q}} \times \boldsymbol{i}_{\hat{d}\hat{q}}) \tag{4}$$

B. MTPA Law

The analytical expression for the MTPA law [7] is derived by differentiating (4) w.r.t the current angle γ for a given current amplitude as in (5).

$$\frac{\mathrm{d}\lambda_d}{\mathrm{d}\gamma} i_q + \lambda_d \frac{\mathrm{d}i_q}{\mathrm{d}\gamma} - \frac{\mathrm{d}\lambda_q}{\mathrm{d}\gamma} i_d - \lambda_q \frac{\mathrm{d}i_d}{\mathrm{d}\gamma} = 0 \tag{5}$$

Incorporating the inductances defined in (3) at $\tilde{\theta} = \tilde{\omega} = 0$, it simplifies to (6).

$$i_d^2\left(L_d - l_q\right) + i_q^2\left(L_q - l_d\right) + 2\,l_{dq}\,i_d\,i_q = 0 \tag{6}$$

The former expression holds significance to the proposed sensorless control as discussed in the later text.

III. Sensorless Control System

The block diagram illustrating an overview of the motor control is shown in the Fig.1.

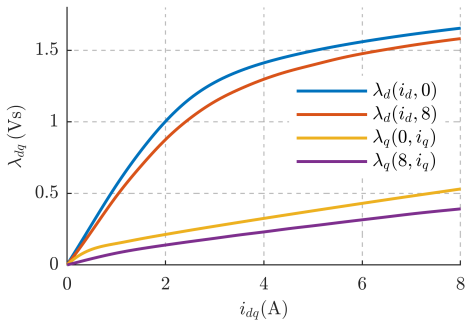

Fig. 2. Experimentally obtained flux maps lookup table, $\boldsymbol{\Lambda}$, of the SyR motor under test: $\boldsymbol{\lambda}_{dq} = \boldsymbol{\Lambda}(\boldsymbol{i}_{dq}) = \boldsymbol{L} \cdot \boldsymbol{i}_{dq}$

A. Flux Observer

The flux observer in stator reference frame is defined by (7) where $\boldsymbol{G}_{\alpha\beta}$ is a 2×2 gain matrix. The estimated stator resistance is denoted by $\hat{R}_s = R_s - \tilde{R}_s$ where $\tilde{R}_s$ is the resistance error. Let $\boldsymbol{\Lambda}$ denote the flux maps lookup table of the machine under test as $\boldsymbol{\lambda}_{dq} = \boldsymbol{\Lambda}(\boldsymbol{i}_{dq})$, shown in the Fig. 2. Then, the estimated inductance $\hat{\boldsymbol{L}}$ is derived as in (8).

$$s\hat{\boldsymbol{\lambda}}_{\alpha\beta} = \hat{\boldsymbol{v}}_{\alpha\beta} - \hat{R}_s \boldsymbol{i}_{\alpha\beta} + \boldsymbol{G}_{\alpha\beta}\left(\mathrm{e}^{\mathbf{J}\hat{\theta}}\,\hat{\boldsymbol{L}}\,\mathrm{e}^{-\mathbf{J}\hat{\theta}}\boldsymbol{i}_{\alpha\beta} - \hat{\boldsymbol{\lambda}}_{\alpha\beta}\right) \tag{7}$$

$$\hat{\boldsymbol{L}}(\boldsymbol{i}_{\hat{d}\hat{q}}) \cdot \boldsymbol{i}_{\hat{d}\hat{q}} = \boldsymbol{\Lambda}(\boldsymbol{i}_{\hat{d}\hat{q}}) \tag{8}$$

In the estimated rotor reference frame, it takes the form in (9) where the gain matrix $\boldsymbol{G}$ equivalence is given by (10).

$$s\,\hat{\boldsymbol{\lambda}}_{\hat{d}\hat{q}} = \hat{\boldsymbol{v}}_{\hat{d}\hat{q}} - \hat{R}_s \boldsymbol{i}_{\hat{d}\hat{q}} - \hat{\omega}\mathbf{J}\,\hat{\boldsymbol{\lambda}}_{\hat{d}\hat{q}} + \boldsymbol{G}\left(\hat{\boldsymbol{L}}\,\boldsymbol{i}_{\hat{d}\hat{q}} - \hat{\boldsymbol{\lambda}}_{\hat{d}\hat{q}}\right) \tag{9}$$

$$\boldsymbol{G} = \mathrm{e}^{-\mathbf{J}\hat{\theta}}\,\boldsymbol{G}_{\alpha\beta}\,\mathrm{e}^{\mathbf{J}\hat{\theta}} \tag{10}$$

For a diagonal matrix $\boldsymbol{G} = g\,\mathbf{I}$, the equivalence $\boldsymbol{G} = \boldsymbol{G}_{\alpha\beta}$ holds.

B. Speed and Position Observer

A conventional phase lock loop (PLL) with a proportional-integral (PI) controller is employed to drive the position error signal ϵ_θ to zero as in (11) where k_p and k_i are the respective gains.

$$\hat{\omega} = k_p\,\epsilon_\theta + \omega_i \qquad \omega_i = \int k_i\,\epsilon_\theta\,\mathrm{d}t \qquad \hat{\theta} = \int \hat{\omega}\,\mathrm{d}t \tag{11}$$

The error signal ϵ_θ is defined as the projection of the difference in observed and current model flux estimates on a projection vector $\boldsymbol{\phi}_\theta$ [8] [9].

$$\epsilon_\theta = \boldsymbol{\phi}_\theta^{\mathrm{T}}\,(\hat{\boldsymbol{\lambda}}_{\hat{d}\hat{q}} - \hat{\boldsymbol{L}}\,\boldsymbol{i}_{\hat{d}\hat{q}}) \tag{12}$$

C. Linearized Error Dynamics

In the interest of studying the stability and susceptibility of observed position to resistance error $\tilde{R}_s$, the error dynamics are linearized for the analytical purposes. The operating point quantities are signified by a subscript 0. The flux error dynamics (13) is derived from (9) where $\tilde{\boldsymbol{\lambda}}_{\hat{d}\hat{q}} = \boldsymbol{\lambda}_{\hat{d}\hat{q}} - \hat{\boldsymbol{\lambda}}_{\hat{d}\hat{q}}$.

$$s\,\tilde{\boldsymbol{\lambda}}_{\hat{d}\hat{q}} = -(\boldsymbol{G}_0 + \omega_0\mathbf{J})\,\tilde{\boldsymbol{\lambda}}_{\hat{d}\hat{q}} + \boldsymbol{G}_0\,(\boldsymbol{\lambda}_{\hat{d}\hat{q}0} - \hat{\boldsymbol{L}}\,\boldsymbol{i}_{\hat{d}\hat{q}0}) - \tilde{R}_s \boldsymbol{i}_{\hat{d}\hat{q}0} \tag{13}$$

Examining the term, $\boldsymbol{\lambda}_{\hat{d}q0} - \hat{\boldsymbol{L}}\,\boldsymbol{i}_{\hat{d}q0}$,

$$\boldsymbol{\lambda}_{\hat{d}q0} - \hat{\boldsymbol{L}}\,\boldsymbol{i}_{\hat{d}q0} = (\boldsymbol{L} - \hat{\boldsymbol{L}})\,\boldsymbol{i}_{\hat{d}q0} + \tilde{\theta}\,(\mathbf{J}\,\boldsymbol{L} - \boldsymbol{L}\,\mathbf{J})\,\boldsymbol{i}_{\hat{d}q0} \tag{14}$$

Although accurate flux maps are assumed, the error in the current model inductance induced by the position error should be accounted for. Considering invariance in incremental inductance [9] gives

$$\boldsymbol{L} \approx \hat{\boldsymbol{L}} + \tilde{\theta}\,(\hat{\boldsymbol{L}} - \boldsymbol{l})\,\mathbf{J} \tag{15}$$

Using the improved inductance model (15) leads to (16a) where $\boldsymbol{\lambda}^{a}_{\hat{d}q0}$, referred as auxiliary flux linkage vector in [8], is defined in (16b).

$$\boldsymbol{\lambda}_{\hat{d}q0} - \hat{\boldsymbol{L}}\,\boldsymbol{i}_{\hat{d}q0} = \tilde{\theta}\,\boldsymbol{\lambda}^{a}_{\hat{d}q0} \tag{16a}$$

$$\boldsymbol{\lambda}^{a}_{\hat{d}q0} = \left(\mathbf{J}\,\hat{\boldsymbol{L}} - \boldsymbol{l}\,\mathbf{J}\right)\boldsymbol{i}_{\hat{d}q0} = \begin{bmatrix}(l_d - \hat{L}_q)\,i_{\hat{q}0} - l_{dq}\,i_{\hat{d}0}\\ (\hat{L}_d - l_q)\,i_{\hat{d}0} + l_{dq}\,i_{\hat{q}0}\end{bmatrix} \tag{16b}$$

Hence, the error dynamics of the system simplifies to

$$s\,\tilde{\boldsymbol{\lambda}}_{\hat{d}q} = -(\boldsymbol{G}_0 + \omega_0\mathbf{J})\,\tilde{\boldsymbol{\lambda}}_{\hat{d}q} + \tilde{\theta}\,\boldsymbol{G}_0\,\boldsymbol{\lambda}^{a}_{\hat{d}q0} - \tilde{R}_s\boldsymbol{i}_{\hat{d}q0} \tag{17}$$

$$\epsilon_{\theta 0} = \boldsymbol{\phi}^{\mathrm{T}}_{\theta 0}\left(\boldsymbol{\lambda}^{a}_{\hat{d}q0}\,\tilde{\theta} - \tilde{\boldsymbol{\lambda}}_{\hat{d}q}\right) \tag{18}$$

If the system is stable, $s\,\tilde{\boldsymbol{\lambda}}_{\hat{d}q} = \epsilon_{\theta 0} = \tilde{\omega} = 0$ holds at steady-state. Upon manipulation, the steady-state position error $\tilde{\theta}_0$ owing to the resistance error $\tilde{R}_s$ is obtained as

$$\tilde{\theta}_0 = -\tilde{R}_s\,\frac{\boldsymbol{\phi}^{\mathrm{T}}_{\theta 0}\left(\boldsymbol{G}_0 + \omega_0\,\mathbf{J}\right)^{-1}\boldsymbol{i}_{\hat{d}q0}}{\boldsymbol{\phi}^{\mathrm{T}}_{\theta 0}\left(\boldsymbol{G}_0 + \omega_0\,\mathbf{J}\right)^{-1}\omega_0\,\mathbf{J}\,\boldsymbol{\lambda}^{a}_{\hat{d}q0}} \tag{19}$$

IV. Active Flux Based Position Estimation

Active flux technique is a state of art flux and position observer for SyR motor drives. The error signal ϵ_θ in the active flux based sensorless control is proportional to the q axis component of $\boldsymbol{\lambda}^{af}_{\hat{d}q}$ in (20).

$$\boldsymbol{\lambda}^{af}_{\hat{d}q} = \hat{\boldsymbol{\lambda}}_{\hat{d}q} - \hat{L}_q\,\boldsymbol{i}_{\hat{d}q} \tag{20}$$

In accordance with former definitions, projection vector for active flux based error signal is given by (21).

$$\boldsymbol{\phi}_{\theta 0} = \frac{1}{\lambda^{a}_{\hat{q}0}}\begin{bmatrix}0\\1\end{bmatrix} \tag{21}$$

For $\boldsymbol{G} = g\mathbf{I}$, the steady-state position error $\tilde{\theta}_0$ (19) simplifies to

$$\tilde{\theta}_0 = \tilde{R}_s\,\frac{\omega_0\,i_{\hat{d}0} - g\,i_{\hat{q}0}}{g\,\omega_0\,\lambda^{a}_{\hat{d}0} + \omega_0^2\,\lambda^{a}_{\hat{q}0}} \tag{22}$$

Fig. 3 presents the $\tilde{\theta}_0$ at $\tilde{R}_s = 0.22$ p.u (1Ω) for $g = 2\pi\cdot 10$ rad/s. Large position error at low speed braking is observed; it is emphasized that the result is derived from the linearized model. Hence, the operating points having $|\tilde{\theta}_0| > 10^\circ$ are likely to be unstable.

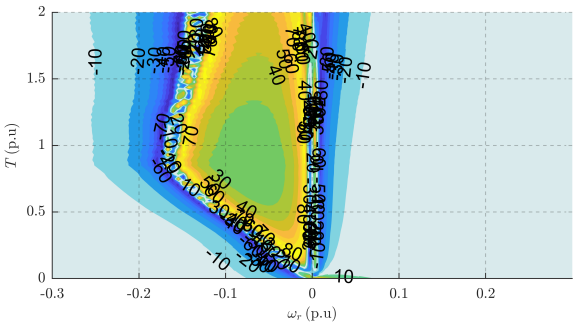

Fig. 3. Steady-state position error in (°) at $\tilde{R}_s = 0.22$ p.u (1Ω) for active flux projection vector at $g = 2\pi\cdot 10$ rad/s (0.2 p.u) on MTPA + i_d^{min} trajectory. Note that the operating points having error greater than $|\tilde{\theta}_0| > 10^\circ$ are likely to be unstable.

V. Proposed Sensorless Technique

A. Adaptive Projection Vector for Position Error Estimation - APP

The proposed projection vector $\boldsymbol{\phi}_\theta$ for position error signal ϵ_θ is

$$\boldsymbol{\phi}^{\mathrm{T}}_{\theta 0} = \begin{bmatrix}0 & \omega_0^{-1}\end{bmatrix}\left(\lambda^{a}_{\hat{d}0}\,\mathbf{I} + \lambda^{a}_{\hat{q}0}\,\mathbf{J}\right)^{-1}\left(\boldsymbol{G}_0 + \omega_0\,\mathbf{J}\right) \tag{23}$$

Substituting in (19), the steady-state position error takes the form in (24).

$$\begin{aligned}\tilde{\theta}_0 &= \frac{\tilde{R}_s}{\omega_0\,|\boldsymbol{\lambda}^{a}_{\hat{d}q0}|^2}\left(\lambda^{a}_{\hat{q}0}\,i_{\hat{d}0} - \lambda^{a}_{\hat{d}0}\,i_{\hat{q}0}\right) \\ &= \frac{\tilde{R}_s}{\omega_0\,|\boldsymbol{\lambda}^{a}_{\hat{d}q0}|^2}\left(i^2_{\hat{d}0}\left(\hat{L}_d - l_q\right) + i^2_{\hat{q}0}\left(\hat{L}_q - l_d\right) + 2\,l_{dq}\,i_{\hat{d}0}\,i_{\hat{q}0}\right)\end{aligned} \tag{24}$$

Examining (24) reveals that it is identical to the MTPA criteria in (6); hence, it concludes that, as long as the MTPA is respected, the proposed projection vector based position observer is immune to errors in stator resistance.

It is worth mentioning that the fundamental component of the voltage error arising due to inverter dead-time is in phase with the stator current vector $\boldsymbol{i}_{\hat{d}q}$ and is reflected in the resistive error term $\tilde{R}_s$. Consequently, immunity also extends towards non-ideal compensation of inverter errors.

B. Combined Stator Resistance and Position Estimation

Although the APP technique is immune to $\tilde{R}_s$ and dead-time on MTPA trajectory, the control deviates from the MTPA for small loads due to the imposition of i_d^{min} for fundamental excitation in sensorless applications. Flux weakening is another case of deviation from MTPA but at high speeds, $\tilde{R}_s$ effects are negligible. Moreover, high performance drives benefit from accurate flux and torque estimation. Hence, a stator resistance adaption is desired.

Akin to the speed observer, a resistance adaption law is defined in (25) where k_r is the gain and ϵ_r is the resistance error signal.

$$\hat{R}_s = k_r\int \epsilon_r\,\mathrm{d}t \qquad \epsilon_r = \boldsymbol{\phi}^{\mathrm{T}}_r\left(\hat{\boldsymbol{\lambda}}_{\hat{d}q} - \hat{\boldsymbol{L}}\,\boldsymbol{i}_{\hat{d}q}\right) \tag{25}$$

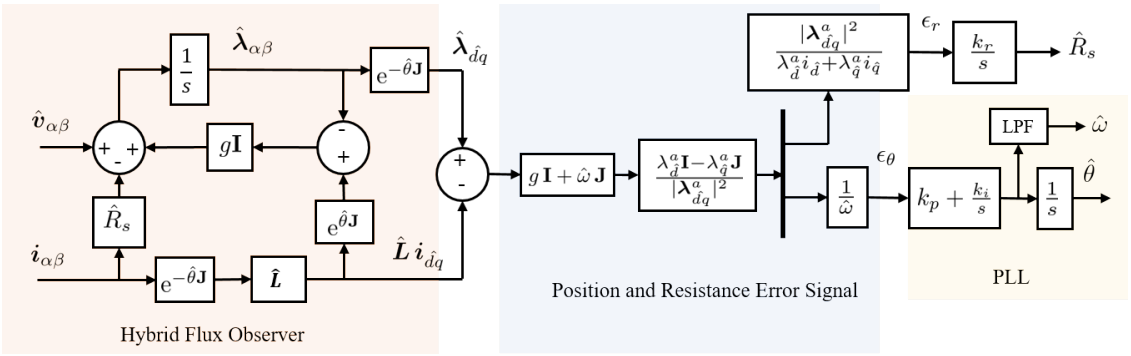

Fig. 4. Hybrid flux observer in stator reference frame with $\boldsymbol{G}^s = \boldsymbol{G} = g\mathbf{I}$, augmented with the APP and stator resistance observer

The cumulative error signal vector $\boldsymbol{\epsilon}$ is given by (26) where the 2×2 projection vector matrix is $\boldsymbol{\Phi} = [\boldsymbol{\phi}_r \quad \boldsymbol{\phi}_\theta]$

$$\boldsymbol{\epsilon} = \begin{bmatrix} \epsilon_r \\ \epsilon_\theta \end{bmatrix} = \boldsymbol{\Phi}^{\mathrm{T}} \left(\hat{\boldsymbol{\lambda}}_{\hat{d}q} - \hat{\boldsymbol{L}}\, \boldsymbol{i}_{\hat{d}q} \right) \tag{26}$$

The position error projection vector $\boldsymbol{\phi}_\theta$ in (23) is retained due to the aforementioned advantages. It is desired that the error signals ϵ_θ and ϵ_r are estimated independently; thus, a natural choice for the resistance error projection vector, $\boldsymbol{\phi}_r$, is a vector orthogonal to $\boldsymbol{\phi}_\theta$ as expressed in (27), where κ is a gain.

$$\boldsymbol{\Phi}_0^{\mathrm{T}} = \begin{bmatrix} \kappa_0 & 0 \\ 0 & \omega_0^{-1} \end{bmatrix} \left(\lambda^a_{\hat{d}0}\, \mathbf{I} + \lambda^a_{\hat{q}0}\, \mathbf{J} \right)^{-1} \left(\boldsymbol{G}_0 + \omega_0\, \mathbf{J} \right) \tag{27}$$

Resorting to the linearized error dynamics to determine κ, using (17) and (18), the cumulative error signal vector $\boldsymbol{\epsilon}_0$ transforms to

$$\begin{bmatrix} \epsilon_{r0} \\ \epsilon_{\theta 0} \end{bmatrix} = \boldsymbol{\Phi}_0^{\mathrm{T}} \left(s\,\mathbf{I} + \boldsymbol{G}_0 + \omega_0\, \mathbf{J} \right)^{-1} \left(\lambda^a_{\hat{d}0}\mathbf{I} + \lambda^a_{\hat{q}0}\mathbf{J} \right) \cdot \left(\begin{bmatrix} s \\ \omega_0 \end{bmatrix} \tilde{\theta} + \frac{\tilde{R}_s}{|\boldsymbol{\lambda}^a_{\hat{d}q0}|^2} \begin{bmatrix} \lambda^a_{\hat{d}0}\, i_{\hat{d}0} + \lambda^a_{\hat{q}0}\, i_{\hat{q}0} \\ \lambda^a_{\hat{d}0}\, i_{\hat{q}0} - \lambda^a_{\hat{q}0}\, i_{\hat{d}0} \end{bmatrix} \right) \tag{28}$$

The gain κ is chosen by equating the steady-state (DC) components of error signal and the resistance error in the absence of position error, i.e., $\epsilon_{r0} = \tilde{R}_s$ at $s = 0$ as $\tilde{R}_s$ is a slow time varying term; it results in

$$\kappa_0 = \frac{|\boldsymbol{\lambda}^a_{\hat{d}q0}|^2}{\lambda^a_{\hat{d}0}\, i_{\hat{d}0} + \lambda^a_{\hat{q}0}\, i_{\hat{q}0}} \tag{29}$$

The steady-state coefficient of $\tilde{R}_s$ in ϵ_{r0}/κ_0 from (28) is shown in Fig. 5.a; it is observed to diminish for low i_q implying that $\tilde{R}_s$ is not observable at these regions. In the contour plot in Fig. 5.b, steady-state coefficient of $\tilde{R}_s$ in $\epsilon_{\theta 0}\,\omega_0$ is shown where the magnitude is minimal near the MTPA trajectory, supporting the claim in (24).

C. Stability Analysis and Gain Selection

Although a comprehensive stability analysis with resistance and position observers is feasible, the two are analyzed independently to gain intuition on the movement of poles at various operating points.

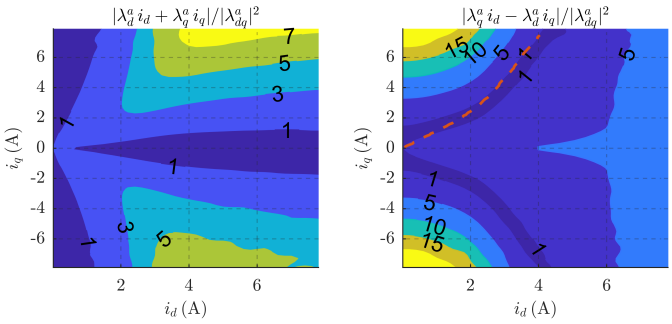

Fig. 5. Effect of $\tilde{R}_s$ on the cumulative error signal $\boldsymbol{\epsilon}$ by examining the coefficients: a) $\frac{\lambda^a_{\hat{d}}\, i_{\hat{d}} + \lambda^a_{\hat{q}}\, i_{\hat{q}}}{|\boldsymbol{\lambda}^a_{\hat{d}q}|^2}$; b) $\frac{\lambda^a_{\hat{d}}\, i_{\hat{q}} - \lambda^a_{\hat{q}}\, i_{\hat{d}}}{|\boldsymbol{\lambda}^a_{\hat{d}q}|^2}$. Red dashed line is the MTPA trajectory.

The error dynamics of the position observer in (11) are shown in (30) where the error signal $\epsilon_{\theta 0}$ is given by (18).

$$s\,\tilde{\theta} = \tilde{\omega}_i - k_p\, \epsilon_{\theta 0} \qquad s\,\tilde{\omega}_i = -k_i\, \epsilon_{\theta 0} \tag{30}$$

The combined dynamics of position and flux observers at $\tilde{R}_s = 0$ is given by (31). At $\boldsymbol{G} = g\,\mathbf{I}$, the eigen values of (31) are a function of ω^2 and are independent of $\boldsymbol{\lambda}^a_{\hat{d}q0}$; the observer is stable for all speeds (barring zero speed).

$$s \begin{bmatrix} \tilde{\boldsymbol{\lambda}}_{\hat{d}q} \\ \tilde{\theta} \\ \tilde{\omega}_i \end{bmatrix} = \begin{bmatrix} -(\boldsymbol{G}_0 + \omega_0\, \mathbf{J}) & \boldsymbol{G}_0\, \boldsymbol{\lambda}^a_{\hat{d}q0} & \mathbf{0} \\ k_p\, \boldsymbol{\phi}^{\mathrm{T}}_{\theta 0} & -k_p\, \boldsymbol{\phi}^{\mathrm{T}}_{\theta 0}\, \boldsymbol{\lambda}^a_{\hat{d}q0} & 1 \\ k_i\, \boldsymbol{\phi}^{\mathrm{T}}_{\theta 0} & -k_i\, \boldsymbol{\phi}^{\mathrm{T}}_{\theta 0}\, \boldsymbol{\lambda}^a_{\hat{d}q0} & 0 \end{bmatrix} \begin{bmatrix} \tilde{\boldsymbol{\lambda}}_{\hat{d}q} \\ \tilde{\theta} \\ \tilde{\omega}_i \end{bmatrix} \tag{31}$$

The gains of PLL are chosen for a critically damped response at $\epsilon_\theta = \tilde{\theta}$ with the poles at $s = -\Omega_\omega = -2\,\pi \cdot 25$ (rad/s).

$$k_p = 2\,\Omega_\omega \qquad k_i = \Omega_\omega^2 \tag{32}$$

The flux observer gain is set to $g = 2\,\pi \cdot 10$ (rad/s) (0.2 pu). Fig. 6.a shows the movement of poles for $\omega = 0.02 \ldots 2$ p.u; the mechanical poles are seen to diverge from the designed Ω_ω at low speeds. Hence, Ω_ω should be sufficiently larger than the poles of speed controller to be adequate at low speeds. This could be circumvented by adapting the flux observer gain matrix $\boldsymbol{G}$ to impose fixed mechanical poles and a desired flux observer poles trajectory [8].

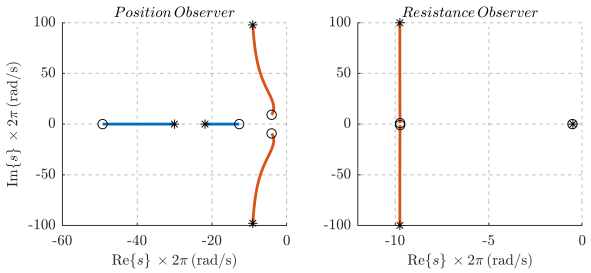

Fig. 6. Locus of poles for $\omega = 0.02 \ldots 2$ p.u where the markers $\circ$ and $*$ denote the speeds 0.02 and 2 p.u respectively: a) Flux and mechanical observer; it is independent of torque and the sign of ω. Mechanical poles are identified in blue and flux observer in red. b) Flux and resistance observer at $T = 1$ p.u.

The combined error dynamics of resistance and flux observer at $\tilde{\theta} = 0$ and $\tilde{\omega}_i = 0$ is given by (33). A low bandwidth of $k_r = 2\,\pi \cdot 0.5$ rad/s is chosen.

$$s \begin{bmatrix} \tilde{\boldsymbol{\lambda}}_{\hat{d}\hat{q}} \\ \tilde{R}_s \end{bmatrix} = \begin{bmatrix} -(\boldsymbol{G}_0 + \omega_0 \mathbf{J}) & -\boldsymbol{i}_{\hat{d}\hat{q}0} \\ k_r\, \boldsymbol{\phi}_{r0}^{\mathrm{T}} & 0 \end{bmatrix} \begin{bmatrix} \tilde{\boldsymbol{\lambda}}_{\hat{d}\hat{q}} \\ \tilde{R}_s \end{bmatrix} \tag{33}$$

The movement of poles at rated torque is shown in the Fig. 6.b. In the vicinity of no load ($i_{\hat{q}} \approx 0$), the poles are seen to delve into the positive plane at low speeds. The condition for stability is determined using Routh-Hurwitz criterion as

$$\omega_0^2 + g_0^2 + \frac{k_r\, g_0}{2} - \frac{k_r\, \omega_0^2}{2 g_0} + \omega_0\, k_r \cdot \frac{\lambda^a_{\hat{q}0}\, i_{\hat{d}0} - \lambda^a_{\hat{d}0}\, i_{\hat{q}0}}{\lambda^a_{\hat{d}0}\, i_{\hat{d}0} + \lambda^a_{\hat{q}0}\, i_{\hat{q}0}} > 0 \tag{34}$$

Hence, the resistance adaptation is disabled for $|T| < 0.2$ p.u. Moreover, owing to poor Signal to Noise Ratio (SNR) at high speeds, it is disabled for $|\omega| > 0.75$ p.u.

VI. Experimental Results

The proposed sensorless scheme is validated experimentally with a 1 kW SyR motor on a dspace DS1103 control platform at a sampling frequency of 10 kHz. A large minimum current of $i_d^{min} = 0.615$ p.u (2A) is imposed to highlight the veracity of resistance observer at non-MTPA operating points. The output of PLL is low pass filtered at a bandwidth of Ω_ω. A PI speed controller with critically damped poles at $s = -2\,\pi \cdot 1$ rad/s is used for close loop control; load torque is imposed by the auxiliary drive connected to the shaft. The parameters of the SyR under test are tabulated in Table I.

TABLE I
Motor Parameters

Parameters	Symbol	Values	Units
Rated Power	P_n	1.1	kW
Rated Voltage	V_n	340	V
Rated Speed	ω_n	1500	rpm
Rated Current	I_n	2.3	A
Rated Torque	T_n	7.1	Nm
Pole pairs	p	2	-
Stator Resistance	R_s	4.5	Ω
Shaft Inertia	J	0.04	kgm^2

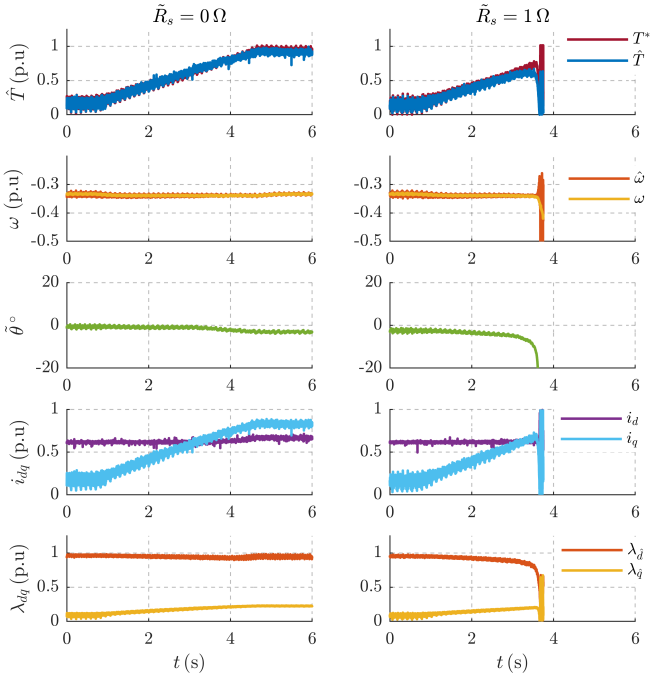

Fig. 7. Susceptibility of Active Flux control on stator resistance variation at $\omega = -0.33$ p.u: a) $\tilde{R}_s = 0\,\Omega$; b) $\tilde{R}_s = 0.22$ p.u $(1\,\Omega)$

A. Instability in Active Flux Control

As highlighted in Fig. 3, the impact of resistance variation on active flux sensorless control is more prominent in the low speed braking regions. However, the active flux control suffers from inherent instability problems in the same region. Hence, the experimental tests, in Fig. 7, are repeated with and without the resistance error for the same operating conditions to ascertain that the loss of control is due to the resistance error. As seen in Fig. 7.b, an error of $\tilde{R}_s = 1\Omega$ results in instability at $\omega = -0.33$ p.u.

B. Immuntity of Proposed Technique to $\tilde{R}_s$

In order to put in evidence the immunity of proposed technique to resistance variation, the $\hat{R}_s$, as seen by the control, is varied by $\pm 100\%$ as shown in the Fig. 8.a at a load torque $T_L = 1$ p.u. where MTPA is respected. Despite the variations in observed flux and torque, the position is undeterred. However, when the MTPA is not respected as in Fig. 8.b at $T_L = 0.5$ p.u, the observed position is susceptible to $\tilde{R}_s$.

C. Stator Resistance Adaptation

The competency of resistance adaption is studied by imposing deliberate variations on the dead-time compensation which is equivalent to physical variations in resistance. A dead-time variation of $\pm 1\mu$s is equivalent to $\pm 3\ \Omega$ at $T = 0.5$ p.u; the equivalence is a function of peak current and changes with load. In Fig. 9.a and b, the effect of changes in dead-time without and with resistance adaption is shown in juxtaposition. With the adaptation, the $\hat{R}_s$ tracks the changes in dead-time

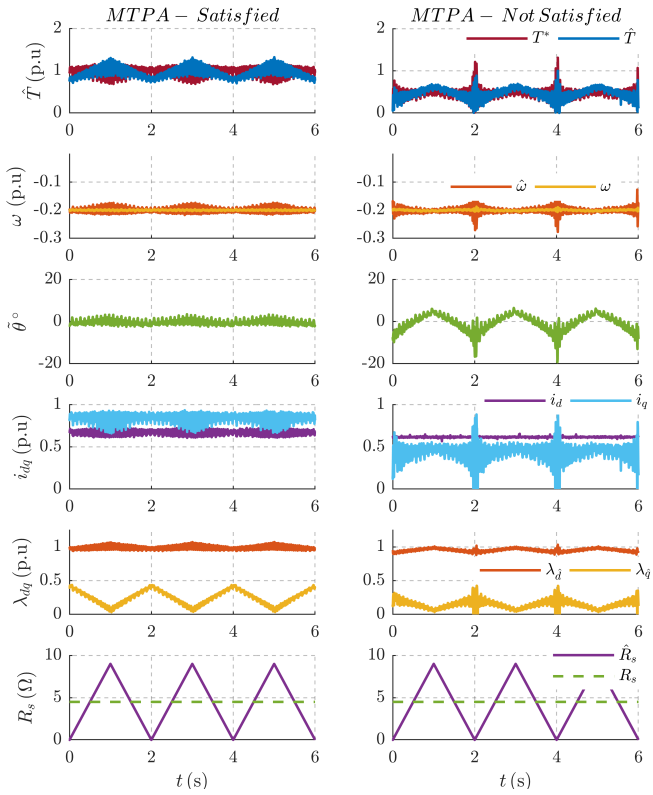

Fig. 8. Immunity of observed position in the APP technique to resistance variation of $\tilde{R}_s = \pm 1$ p.u ($\pm 4.5\Omega$): a) $T_L = 1$ p.u, on MTPA trajectory; b) $T_L = 0.5$ p.u, away from MTPA due to i_d^{min}.

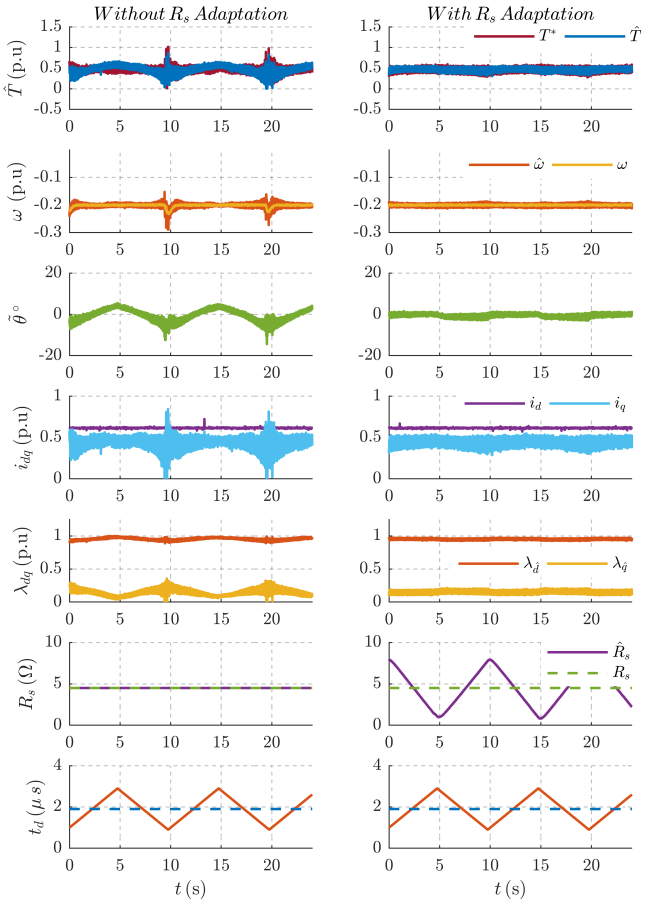

Fig. 9. Variations on dead-time compensation ($\pm 1\mu s$) to emulate $\tilde{R}_s$ at $T_L = 0.5$ p.u and $\omega = -0.2$ p.u: a) Without R_s adaptation; b) With R_s adaptation.

and thereby alleviates the impact on observed position, stator flux and torque.

VII. Conclusion

A generic framework for the analysis of stator resistance variation was presented, whereupon the effect on active flux control was studied and instability regions at low speed braking were identified. The immunity of proposed projection vector for MTPA operating points was discussed. In the interest of extending the immunity to non-MTPA operating points as well as for accurate estimation of stator flux and torque, a resistance adaption law was designed wherein the resistance error signal is orthogonal and independent of position error signal. Stability analysis was performed to sketch the movement of poles and to calibrate observer gains. The instability of active flux and the proposed techniques were experimentally evaluated on a 1.1 kW SyR machine test bench.

References

[1] F. Briz and M. W. Degner, "Rotor Position Estimation," *IEEE Industrial Electronics Magazine*, vol. 5, no. 2, pp. 24–36, 2011.

[2] S. C. Agarlita, I. Boldea, and F. Blaabjerg, "High-frequency-injection-assisted 'active-flux'-based sensorless vector control of reluctance synchronous motors, with experiments from zero speed," *IEEE Transactions on Industry Applications*, vol. 48, no. 6, pp. 1931–1939, 2012.

[3] M. Hinkkanen, T. Tuovinen, L. Harnefors, and J. Luomi, "A Combined Position and Stator-Resistance Observer for Salient PMSM Drives: Design and Stability Analysis," *IEEE Transactions on Power Electronics*, vol. 27, no. 2, pp. 601–609, 2012.

[4] D. Liang, J. Li, and R. Qu, "Sensorless Control of Permanent Magnet Synchronous Machine Based on Second-Order Sliding-Mode Observer With Online Resistance Estimation," *IEEE Transactions on Industry Applications*, vol. 53, no. 4, pp. 3672–3682, 2017.

[5] Y. Inoue, Y. Kawaguchi, S. Morimoto, and M. Sanada, "Performance Improvement of Sensorless IPMSM Drives in a Low-Speed Region Using Online Parameter Identification," *IEEE Transactions on Industry Applications*, vol. 47, no. 2, pp. 798–804, 2011.

[6] I. R. Bojoi, E. Armando, G. Pellegrino, and S. G. Rosu, "Self-commissioning of inverter nonlinear effects in AC drives," *2012 IEEE International Energy Conference and Exhibition, ENERGYCON 2012*, pp. 213–218, 2012.

[7] A. Varatharajan, S. S. Cruz, H. Hadla, and F. Briz, "Predictive torque control of SynRM drives with online MTPA trajectory tracking and inductances estimation," in *Electric Machines and Drives Conference (IEMDC), 2017 IEEE International*, 2017, pp. 1–7.

[8] M. Hinkkanen, S. E. Saarakkala, H. A. A. Awan, E. Molsa, and T. Tuovinen, "Observers for Sensorless Synchronous Motor Drives: Framework for Design and Analysis," *IEEE Transactions on Industry Applications*, p. 1, 2018.

[9] A. Varatharajan and G. Pellegrino, "Sensorless Control of Synchronous Reluctance Motor Drives : Improved Modeling and Analysis beyond Active Flux," in *Electric Machines and Drives Conference (IEMDC), IEEE International*, 2019 (In Press).